

The fabrication of high density nanochannel organic light emitting diodes with reduced charge spreading

K Trivedi¹, U S Bhansali², B Gnade² and W Hu¹

¹ Department of Electrical Engineering, University of Texas at Dallas, Richardson, TX 75080, USA

² Department of Material Science and Engineering, University of Texas at Dallas, Richardson, TX 75080, USA

E-mail: walter.hu@utdallas.edu

Received 11 April 2009, in final form 21 July 2009

Published 8 September 2009

Online at stacks.iop.org/Nano/20/405204

Abstract

This study reports fabrication and characterization of nanoscale organic light emitting diodes with reduced charge spreading. Nanoimprint lithography is used to make *SU-8* nanochannels with $\sim 90^\circ$ sidewalls into which *N'*-bis(naphthalen-1-yl)-*N,N'*-bis(phenyl)benzidine (NPB) and tris-(8-hydroxyquinoline) aluminum (Alq_3) are thermally evaporated, to avoid charge spreading. Micron grating devices are fabricated for comparison. Device characteristics show that performance is retained while scaling down to nanochannels, as no geometry dependent trend is observed. Surface potential microscopy (SPM) measurements reveal an identical periodic difference in surface potential for nanochannel and microscale grating devices. The SPM results, together with cross-sectional scanning electron microscopy observation of the physical separation of nanoscale organic light emitting diodes (OLEDs), indicate electrical separation and isolated light emission from nanoscale confined OLEDs with minimized charge spreading.

(Some figures in this article are in colour only in the electronic version)

1. Introduction

Nanoscale light sources are required for applications in bio-sensing, high density data storage, near-field optical lithography and nanophotonic devices [1–4]. In particular, lithographically defined nanochannel light emitting arrays can be applied toward near-field bio-sensing, lab-on-chip as well as all-organic photonic circuits [5]. Most inorganic light emitting semiconductors are not suitable for miniaturization down to nanoscale due to limitations in electrical and optical characteristics resulting from geometry dependent band structure and fabrication challenges [6–9]. Chemically grown InP nanowires have been shown to output light by devices formed on a random orientation of nanowires; however, the effective emissive area remains significantly larger than the nanowire dimension and the nanowires are grown at temperatures as high as 850°C [10, 11]. The conditions and challenges associated with fabrication of inorganic nanowires make such devices inapplicable to applications

requiring low-temperature processing or lithographically defined control. Organic light emitting diodes (OLEDs) are a viable alternative for miniaturization as they are well researched and offer relatively uncomplicated, low-cost and low-temperature fabrication. Moreover, electrical and optical characteristics of miniaturized OLED devices are not bound by quantum confinement, due to the amorphous structure of the active organic materials in which charge transport occurs by carrier hopping [12–15].

Previous studies have demonstrated that OLEDs can be patterned by a variety of techniques including photolithography and soft lithography [16–19]. In these studies, the cathode or anode was patterned down to several micrometers and the resultant light emission area was even larger due to charge spreading in the active layer. To minimize charge spreading, in an effort to make discrete sub-micrometer OLED pixels, more recent approaches have relied on electron beam and nanoimprint lithography (NIL) techniques to attempt to isolate the active materials in between insulating

materials such as silicon dioxide, silicon nitride, poly(methylmethacrylate) and polystyrene [20–24]. These studies show the viability of patterning active OLED materials in an insulating layer to produce light from sub-micron scale pixels. However, thus far, all approaches to fabricate such devices utilize processes which ultimately lead to charge spreading in the hole injection material or avoid using a hole transport layer at all. One popular hole injection material is poly(3,4-ethylenedioxythiophene):poly(styrenesulfonate) or PEDOT:PSS, which, after spin-coating, forms a conformal coating on insulating features rather than forming discrete active patterns. As suggested by Lidzey *et al*, conformal coating leads to charge spreading in the PEDOT layer, causing the effective emissive area to be larger than the patterned gap in the insulating features [20]. Such charge spreading can defeat the most elaborate scheme to scale OLED devices to nanoscale. Another obstacle is the fundamental limit of conventional optical imaging techniques which have a resolution on the order of about $0.5 \mu\text{m}$, making it difficult to obtain direct optical evidence of nanoscale light emission.

An alternative approach to confirm isolated light emission is to show electrical separation of the active materials as deposited into the nanoscale features. Electrical separation would prevent charge spreading, leading to discrete emission from nanoscale features. Thus far, neither physical nor electrical separation of active material inside the nanocavities has been shown. Surface potential microscopy (SPM), also referred to as contact potential or kelvin probe force microscopy is a powerful technique to determine surface electrical properties [25, 26]. A difference in surface potential infers a difference in electric field and surface work function as a result of non-uniform charge distribution. Surface potential microscopy has been utilized to study electrostatic potential across organic films as well as organic transistor devices [27–29]. Recently, this technique has been used to detect the local surface work function in organic solar cells to determine morphologically dependent charge transport properties of the devices as well as work function of ITO surfaces used in OLED fabrication [30, 31].

In this study, we demonstrate the highest density (5×10^4 channels cm^{-1}) nanochannel confined OLEDs reported to date, fabricated with a simple low-temperature NIL process. Small molecule materials are thermally evaporated into *SU-8* trenches fabricated with an optimized process to result in $\sim 90^\circ$ sidewalls. The vertical sidewalls of the trenches together with use of thermally evaporated materials leverage shadowing for non-conformal deposition of active layers, thereby leading to reduced charge spreading. Both nanochannel and micrometer scale (fabricated for comparison) devices are characterized by electrical and optical measurements, as well as SPM. Device characteristics show no geometry dependence, suggesting organic light sources can be scaled down to nanoscale without impact on performance characteristics. SPM reveals an identical periodic difference in surface potential for both nanochannel and microscale grating devices. The SPM results together with cross-sectional SEM observation of physical separation of active materials in nanochannel OLEDs indicate electrical separation of individual nanochannels which should

reduce charge spreading. This study, together with previous reports, suggests that OLED devices are suitable for confined nanoscale light output.

2. Experimental details

Indium tin oxide (ITO) coated glass (Delta Technologies) served as OLED device substrates. Identical devices were fabricated on silicon for cross-sectional SEM imaging of the device stack. The substrates were cleaned in acetone and isopropyl alcohol, treated with oxygen plasma and patterned by photolithography to define separate device areas. Nanochannel OLED devices with line and space gratings (100 nm each) were defined in *SU-8* photo-resist on top of the patterned ITO by NIL as shown in figure 1. A stable insulating material such as *SU-8* is required, as low contrast of OLED pixels has previously been attributed to intermixing of the active polymer layers with low glass transition temperature insulating material due to heating during device operation [21]. *SU-8* is expected to be stable during device operation as it has a post-crosslink glass transition temperature of over 200°C . In addition to having superior post-crosslink insulating and mechanical properties, it offers easy, low-temperature fabrication ($55\text{--}85^\circ\text{C}$) by NIL. The *SU-8* was imprinted with a silicon mold (Nanonex), containing a large area of 100 nm line and space gratings with an average depth of 95 nm (figure 2(a)). The mold was treated with perfluorodecyltrichlorosilane (FDTS) to prevent adhesion of *SU-8* to the mold during imprint. The imprinted *SU-8* patterns were cured under UV (450 mJ cm^{-2}) and baked to facilitate cross-linking of *SU-8*. It has been shown that by calibrating the initial spin-coated polymer thickness prior to NIL, it is possible to achieve a residue layer with variable thickness [34]. The initial film thickness must be calibrated for both density and depth of the mold. For our mold, having a density of 50% and an average depth of 95 nm, we found an initial spin-coated *SU-8* film thickness of 95 nm results in uniform 75–85 nm tall features with a residue layer of 30 nm over an area of 4 cm^2 (figure 2(b)). Thickness of the residue layer increases with initial film thickness. Therefore, it is possible to control final *SU-8* structure height after residue etching without changing the mold height. To expose ITO between *SU-8* gratings, the residue layer must be etched while maintaining overall grating profile integrity. However, etching of the residue layer without protecting the imprinted features would result in a decrease in pattern height as well as rounding of the top surface of the imprinted features [17] which could lead to conformal coating of the active materials. To selectively etch the residue layer, a hard masked residue etching process was developed using oblique angle evaporation of chromium (Cr) (figure 1(c)) at an angle of 10° , which allows selective coating of metal only on the top surfaces of *SU-8* gratings. Figure 2(b) shows a SEM micrograph of imprinted patterns after oblique angle Cr deposition. The residue layer was etched in an inductively coupled oxygen plasma (5 mTorr, 25°C , 300 W ICP power, 100 W bias power). The samples were etched for 10 s to account for any non-uniformity in the residue layer, assuring complete residue removal. The bulk of the residue is likely etched away in approximately 3 s

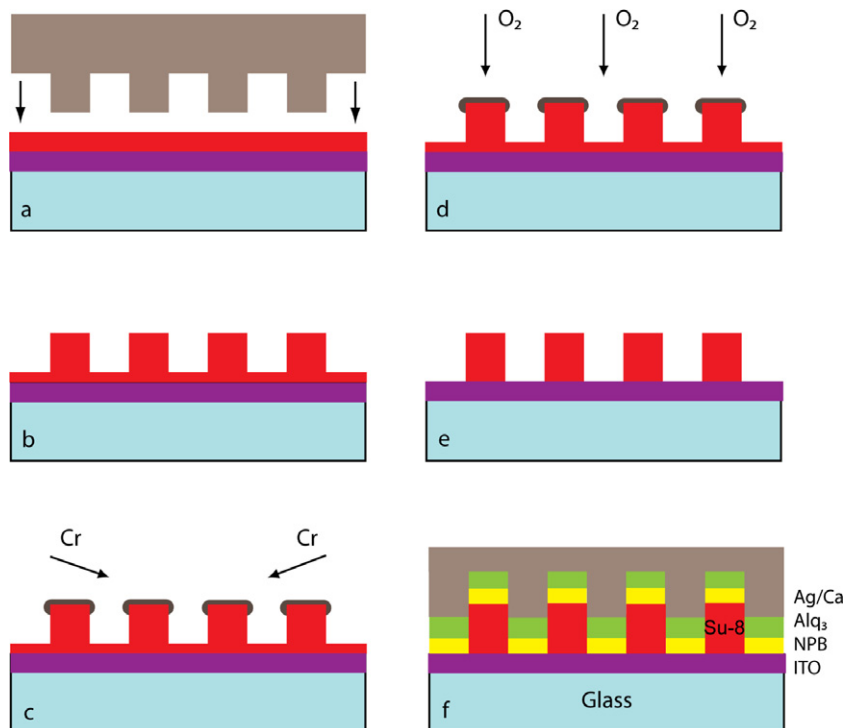


Figure 1. Nanochannel OLED process flow (a) Si mold is pressed into the *SU-8* film on ITO coated glass; (b) the mold is removed, leaving imprinted *SU-8* gratings; (c) Cr is coated on top of the imprinted *SU-8* gratings at an oblique angle; (d) the residue is etched by O_2 plasma, with the Cr protecting the *SU-8* gratings; (e) the imprinted *SU-8* gratings are isolated after O_2 plasma etch; (f) organics and metal are deposited by thermal evaporation.

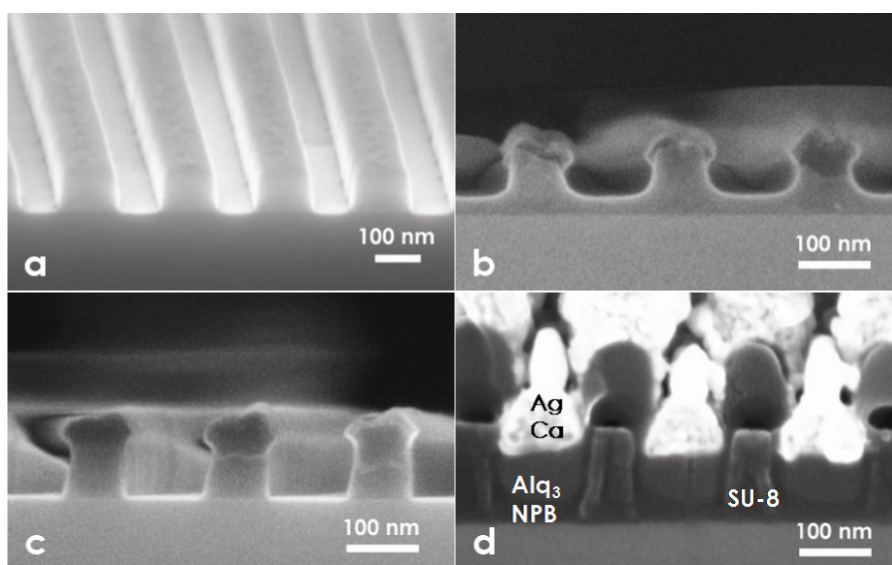


Figure 2. SEM micrographs showing cross sections of (a) the Si mold used to imprint the *SU-8*; (b) imprinted *SU-8* gratings after oblique angle Cr evaporation; (c) isolated *SU-8* gratings with Cr on top after O_2 plasma etch; (d) a typical nanochannel OLED device after thermal evaporation of organics and metal.

while the ITO is further cleaned by the oxygen plasma for the remainder of the etch. Figure 2(c) shows a SEM micrograph of the imprinted *SU-8* patterns after residue etch, with Cr remaining on top of the patterns. After residue etching, the samples undergo a 2 min wet etch to remove the Cr mask, leaving only isolated *SU-8* nanochannel gratings with ITO

exposed between gratings. This process produces rectangular gratings with sharp and vertical sidewalls, which is expected to prevent highly conformal coating during thermal evaporation of organics. In addition to nanochannel *SU-8* gratings, we fabricated micrometer scale *SU-8* line and space patterns with dimensions of 2, 5 and 10 μm by a standard photolithography

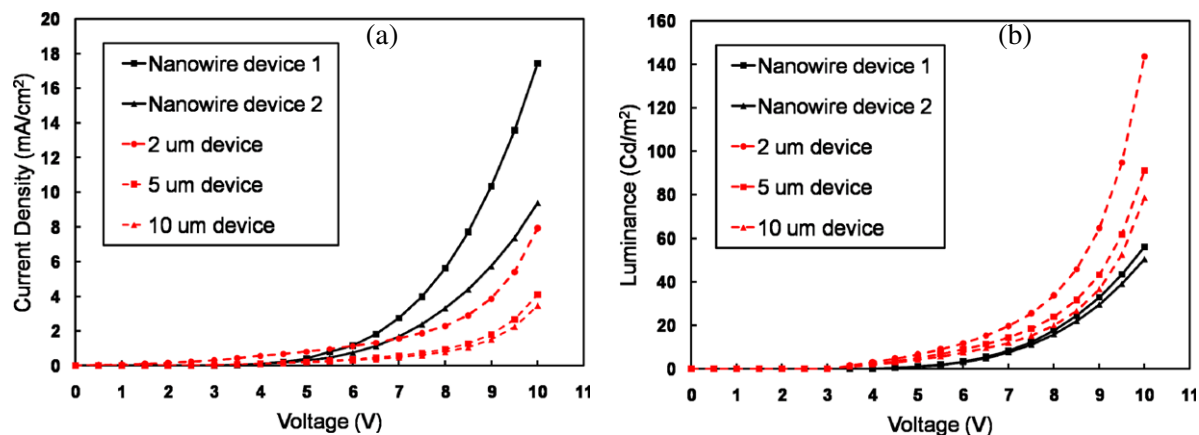


Figure 3. Electrical characterization data showing (a) current density versus voltage characteristics; and (b) luminance versus voltage characteristics of microscale and nanochannel OLED devices.

process. Initial film thickness was calibrated to yield *SU*-8 gratings with the same height as nanochannel gratings.

Next, *N,N'*-bis(naphthalen-1-yl)-*N,N'*-bis(phenyl)benzidine (NPB), tris-(8-hydroxyquinoline) aluminum (Alq₃), calcium (Ca), and silver (Ag) were deposited into the nanochannel and microscale *SU*-8 gratings by thermal evaporation, which is expected to produce uniform but more non-conformal filling in the *SU*-8 nanotrenches without significant sidewall coating. Even in the worst case of conformal coating, it has been suggested that charge spreading can be minimized, if not eliminated, by replacing polymeric materials such as PEDOT:PSS with materials having a higher resistivity or lower hole mobility [20]. The hole mobility in NPB is an order of magnitude lower (10^{-3} – 10^{-4} cm² V⁻¹ s⁻¹) compared to PEDOT:PSS (10^{-2} – 10^{-3} cm² V⁻¹ s⁻¹) [32, 33]. For all devices, 30 nm of NPB was deposited, followed by 75 nm of Alq₃, 50 nm of Ca and 100 nm of Ag. The thickness of the individual organic materials inside the nanochannel gratings was carefully calibrated, as it can be vastly different from blanket deposition, which is used in conventional OLED device fabrication. Significant shadowing, caused by angled incident flux of organics inside the high aspect ratio trenches of nanochannel devices can occur during thermal evaporation as material is deposited in between and on top of the *SU*-8 gratings, resulting in non-uniform coating inside trenches. Consequently, the effect of shadowing increases as more material is deposited on top of the *SU*-8 gratings, as there is an effective increase in the aspect ratio of the trenches. Problematic shadowing can be alleviated by holding the substrates stationary over the organic sources during thermal evaporation. Devices fabricated on silicon, with identical nanochannel patterns, are placed alongside devices made on ITO coated glass during thermal evaporation in order to examine the filling inside the gratings with cross-sectional SEM. Figure 2(d) shows a SEM micrograph of a typical nanochannel OLED device. The organics are deposited in the trenches as well as on top of the *SU*-8 gratings. However, in contrast to spin-coated active materials, the organic materials are deposited in a highly non-conformal manner, with a negligible amount of material on the sidewalls, indicating the light emitting materials are physically confined and separated in the *SU*-8 nanochannels.

3. Results and discussion

All devices underwent electrical and optical characterization with a Keithley 2400 power supply and a photoresearch PR-650 Spectra Photometer interfaced with Labview. The OLED devices were biased from 0 to 10 V and the current density and luminance (cd m⁻²) were measured simultaneously. Figure 3 shows the electrical and optical characteristics of nanochannel and microscale OLED devices fabricated on ITO coated glass. As seen in figure 3(a), the current density of nanochannel OLED devices is observed to be higher than that of microscale devices. Higher current density in nanochannel devices could be attributed to the close proximity of the metal to the NPB layer inside the nanochannels (figure 2(d)), which could lead to non-radiative recombination and increased current. The greater number of channels in nanochannel devices compared to microscale grating devices would amplify this effect. Even so, the recorded current density for our nanochannel OLED devices is lower than the current density reported by previous studies attempting to fabricate nanoscale OLED pixels [22]. Current in OLED devices is dependent on various parameters such as materials used and active layer thickness but lower current density in our nanochannel OLED devices could be attributed to reduction of charge spreading by successful isolation of light emitting trenches from non-emitting *SU*-8 gratings, which is desired for discrete nanoscale light sources. Figure 3(b) shows luminance of microscale grating devices to be higher than the nanochannel OLED devices. In channeled devices (both microscale and nanoscale), the non-emissive *SU*-8 regions separating the emissive channels do not contribute to luminescence. Therefore, the total emissive area in our devices is half that of a device with no *SU*-8 insulating features (large scale standard OLED). This effective area is used in the calculation of luminance of all devices in figure 3(b). The data shows that light output from the 2 μm grating device is not only brighter than the 5 and 10 μm grating devices, but the nanochannel devices as well. Hence, there is no clear geometry dependence in the brightness of OLED devices of varying grating size. At low bias, the nanochannel devices exhibited slightly lower brightness than the microscale grating devices while having

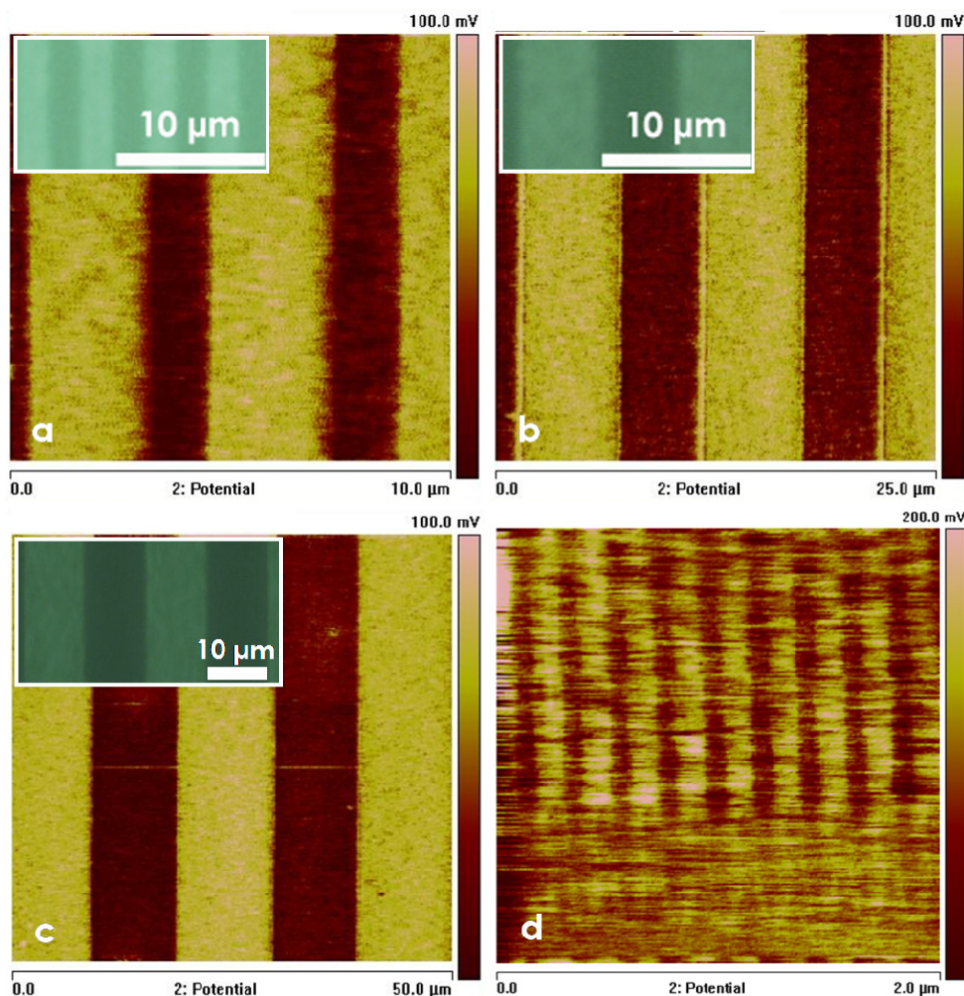


Figure 4. Surface potential micrographs with insets showing light emission profile under optical microscope of (a) 2 μm grating; (b) 5 μm grating; (c) 10 μm grating; and (d) nanochannel OLED devices.

a higher current density. However, nanochannel devices were brighter than microscale grating devices at higher current densities, beyond an applied bias of 10 V, reaching luminescence values exceeding 1000 cd m^{-2} at 15 V. Hence, the observed higher current density paired with relatively lower luminescence at low bias are not related to scaling down of the dimension of light emitting trenches. The difference in current density between the two nanochannel devices could be due to degradation, as the OLED devices are uncapsulated. The process flow and conditions can certainly be optimized for better device performance. Previous studies attempting to fabricate nanoscale OLEDs document similar performance or omit device electrical and optical characterization data altogether [20, 21, 24]. The electrical and optical characterization data of the nanochannel OLEDs show no geometry dependence and, therefore, indicate that miniaturization of OLEDs to nanoscale would result in similar performance as microscale devices, which makes them feasible as nanoscale light sources for near-field applications.

SPM was performed under ambient conditions with white light on both microscale and nanochannel OLED devices without metal cathodes. Metal was not deposited so that the

surface of the organics can be scanned across the morphology of the devices. A Veeco Dimension V atomic force microscope system was set up for amplitude modulation (AM mode) SPM with a conductive 1Ω silicon tip having a spring constant of 40 N m^{-1} . An a.c voltage of 4 V was superimposed on the tip, while a d.c voltage of 8 V was applied to the sample, which caused the tip to oscillate in response to the electrostatic forces on the surface of the sample. During the surface potential scan, the tip is held 5 nm above the surface of the sample as the surface potential is recorded. In a closed loop system like ours, for every line scanned, surface topography is first recorded immediately before the SPM scan and is used as a reference in the active feedback process to maintain a certain distance between the tip and the sample surface. Figure 4 shows SPM micrographs of the surface potential across several gratings of the microscale and nanochannel OLED devices as well as light emission profiles taken under an optical microscope (insets). The change in surface potential corresponds to the grating topography. A distinct difference in the surface potential on top of the SU-8 gratings and the trenches is immediately visible. In all devices, a higher surface potential is observed on top of the SU-8 structures, indicating a non-uniform charge

Table 1. Recorded average difference in surface potential of organics on top of SU-8 gratings and inside trenches.

Grating dimension	Average ΔSP
10 μm gratings	64 mV
5 μm gratings	63 mV
2 μm gratings	68 mV
100 μm gratings	65 mV

distribution between the top of the SU-8 gratings and the trenches. Table 1 shows the same recorded average difference in surface potential (ΔSP) of organics on top of SU-8 gratings and inside trenches for all devices, regardless of geometry. The slight reduction in contrast and image quality for nanochannel gratings (figure 4(d)) is expected in AM mode as it is carried out in ambient conditions. More importantly, long range electrostatic forces affect the readings in AM mode, making it difficult to differentiate changes in surface potential that are too closely-spaced. It has been reported that actual surface potential can be as much as 4 times greater than AM mode readings [25]. Therefore, the real ΔSP in our devices may well be higher than our measurements. The SPM measurements presented show a periodic difference in surface potential of organics inside trenches and on top of SU-8 gratings. This distinct periodic difference in surface potential could be attributed to electrical separation of the organic stacks inside trenches and on top of the SU-8 gratings. Furthermore, electrical separation of organic stacks is evident in the light emission profiles of microscale grating devices (insets of figures 4(b)–(d)). Light output is observed only from the trenches, indicating confinement of recombination within the organics inside trenches. It is apparent from the light emission profiles of microscale grating devices that charge spreading is not a problem in devices fabricated only with thermally evaporated NPB Alq3 inside vertical SU-8 gratings. Unfortunately, due to diffraction limitations of optical microscopy similar discrete light emission profile from nanochannel OLED devices cannot be observed directly. Nevertheless, the similar ΔSP observed in the microscale and nanochannel OLED devices indicates that light emission profile of nanochannel OLED devices should also be discrete with light output only from the nanoscale trenches in between the SU-8 gratings, much like light emission from microscale devices.

4. Conclusion

In summary, we have demonstrated and characterized high density nanochannel OLED devices using thermally evaporated small molecule materials deposited into insulating SU-8 gratings. The optimized fabrication process with vertical SU-8 sidewalls and thermal evaporation of active layers allows fabrication of nanochannel OLEDs with minimal charge spreading. The process is well controlled and allows for a low-temperature NIL based fabrication compatible with organic devices. Cross-sectional SEM observation has shown physical confinement and separation of light emitting materials in the nanochannels. Device characteristics show no geometry

dependence, suggesting nanochannel OLEDs can be scaled down while retaining performance characteristics. A surface potential microscopy technique is developed to show identical electrical separation of organics deposited inside trenches and on top of SU-8 gratings in both microscale and nanochannel OLED devices. Light emission profiles of microscale grating devices show that the measured ΔSP can be correlated with discrete light emission from the microtrenches. The identical ΔSP observed for both microscale and nanochannel OLED devices indirectly suggests identical isolated light emission from the nanotrenches in the nanochannel OLED devices. The developed method presents a highly adaptable, well controlled, low-temperature process for fabricating nanoscale light sources capable of confined light output with reduced charge spreading.

Acknowledgment

This work is supported by the Air Force Office of Scientific Research through the SPRING program (No. FA9550-06-1-0403).

References

- [1] Terris B D, Mamin H J and Rugar D 1996 *Appl. Phys. Lett.* **68** 141–3
- [2] Yuan Z L, Kardynal B E, Stevenson R M, Shields A J, Lobo C J, Cooper K, Beattie N S, Ritchie D A and Pepper M 2002 *Science* **295** 102–5
- [3] Cacialli F, Riehn R, Downes A, Latini G, Charas A and Morgado J 2004 *Ultramicroscopy* **100** 449–55
- [4] Ohtsu M, Kobayashi K, Kawazoe T, Sangu S and Yatsui T 2002 *IEEE J. Sel. Top. Quantum Electron.* **8** 839–62
- [5] Tegenfeldt J O, Prinz C, Cao H, Huang R L, Austin R H, Chou S Y, Cox E C and Sturm J C 2004 *Anal. Bioanal. Chem.* **378** 1678–92
- [6] Gilliland G D 1997 *Mater. Sci. Eng. R* **18** 99–399
- [7] Fiore A, Chen J X and Ilegems M 2002 *Appl. Phys. Lett.* **81** 1756–8
- [8] Fukui T, Ando S, Tokura Y and Toriyama T 1991 *Appl. Phys. Lett.* **58** 2018–20
- [9] Fiore A et al 2001 *IEEE J. Quantum Electron.* **37** 1050–8
- [10] Duan X F, Huang Y, Cui Y, Wang J F and Lieber C M 2001 *Nature* **409** 66–9
- [11] Gudiksen M S, Lauhon L J, Wang J, Smith D C and Lieber C M 2002 *Nature* **415** 617–20
- [12] Sirringhaus H et al 1999 *Nature* **401** 685–8
- [13] Wolf U, Arkhipov V I and Bassler H 1999 *Phys. Rev. B* **59** 7507–13
- [14] Arkhipov V I, Wolf U and Bassler H 1999 *Phys. Rev. B* **59** 7514–20
- [15] Barth S, Wolf U, Bassler H, Muller P, Riel H, Vestweber H, Seidler P F and Riess W 1999 *Phys. Rev. B* **60** 8791–7
- [16] Granlund T, Nyberg T, Roman L S, Svensson M and Inganas O 2000 *Adv. Mater.* **12** 269–73
- [17] Koide Y, Wang Q W, Cui J, Benson D D and Marks T J 2000 *J. Am. Chem. Soc.* **122** 11266–7
- [18] Lidzey D G, Pate M A, Weaver M S, Fisher T A and Bradley D D C 1996 *Synth. Met.* **82** 141–8
- [19] Renak M L, Bazan G C and Roitman D 1997 *Adv. Mater.* **9** 392
- [20] Boroumand F A, Fry P W and Lidzey D G 2005 *Nano Lett.* **5** 67–71
- [21] Cheng X, Hong Y T, Kanicki J and Guo L J 2002 *J. Vac. Sci. Technol. B* **20** 2877–80

- [22] Suh D and Lee H H 2004 *J. Vac. Sci. Technol. B* **22** 1123–6
- [23] Veinot J G C, Yan H, Smith S M, Cui J, Huang Q L and Marks T J 2002 *Nano Lett.* **2** 333–5
- [24] Yamamoto H, Wilkinson J, Long J P, Bussman K, Christodoulides J A and Kafafi Z H 2005 *Nano Lett.* **5** 2485–8
- [25] Glatzel T, Sadewasser S and Lux-Steiner M C 2003 *Appl. Surf. Sci.* **210** 84–9
- [26] Sommerhalter C, Glatzel T, Matthes T W, Jager-Waldau A and Lux-Steiner M C 2000 *Appl. Surf. Sci.* **157** 263–8
- [27] Burgi L, Sirringhaus H and Friend R H 2002 *Appl. Phys. Lett.* **80** 2913–5
- [28] Nichols J A, Gundlach D J and Jackson T N 2003 *Appl. Phys. Lett.* **83** 2366–8
- [29] Yamada H, Fukuma T, Umeda K, Kobayashi K and Matsushige K 2002 *Appl. Surf. Sci.* **188** 391–8
- [30] Chen S H 2005 *J. Appl. Phys.* **97** 073713
- [31] Hoppe H, Glatzel T, Niggemann M, Hinsch A, Lux-Steiner M C and Sariciftci N S 2005 *Nano Lett.* **5** 269–74
- [32] Bernards D A and Malliaras G G 2007 *Adv. Funct. Mater.* **17** 3538–44
- [33] Hung L S and Chen C H 2002 *Mater. Sci. Eng. R* **39** 143–222
- [34] Al-Assaad R M, Regonda S, Tao L, Pang S W and Hu W W 2007 *J. Vac. Sci. Technol. B* **25** 2396–401